AIMS Materials Science, 2(4): 392-400.
DOI: 10.3934/matersci.2015.4.392
Received date 24 August 2015,
Accepted date 20 October 2015,
Published date 22 October 2015

http://www.aimspress.com/

Research article

Magnetic properties of Sm_5Fe_{17} melt-spun ribbons and their borides

Tetsuji Saito [1,*] and Daisuke Nishio-Hamane [2]

[1] Department of Mechanical Science and Engineering, Chiba Institute of Technology, 2-17-1 Tsudanuma, Narashino, Chiba 275-0016, Japan
[2] Institute for Solid State Physics, The University of Tokyo, 5-1-5 Kashiwanoha, Kashiwa, Chiba 277-8581, Japan

* **Correspondence:** Email: tetsuji.saito@it-chiba.ac.jp; Tel: +81-47-478-0315; Fax: +81-47-478-0329.

Abstract: Sm_5Fe_{17} melt-spun ribbons exhibited low coercivity and partly or mostly consisted of the amorphous phase. Annealing of Sm_5Fe_{17} melt-spun ribbon resulted in the formation of the Sm_5Fe_{17} phase. The annealed Sm_5Fe_{17} melt-spun ribbon exhibited a high coercivity. It was found that the addition of B to the Sm_5Fe_{17} alloy resulted in the promotion of the $Sm_2Fe_{14}B$ phase. Annealed $Sm_5Fe_{17}B_x$ (x = 0.5) melt-spun ribbons consisted of the Sm_5Fe_{17} phase together with the $Sm_2Fe_{14}B$ and $SmFe_2$ phases. On the other hand, annealed $Sm_5Fe_{17}B_x$ (x = 1.0–1.5) melt-spun ribbons consisted of the $Sm_2Fe_{14}B$ and $SmFe_2$ phases without the Sm_5Fe_{17} phase. The resultant $Sm_5Fe_{17}B_x$ (x = 1.0–1.5) melt-spun ribbons still showed a coercivity of around 2 kOe. The annealed Sm_5Fe_{17} melt-spun ribbon exhibited a high coercivity over 25 kOe and a remanence of 40 emu/g, whereas the annealed $Sm_5Fe_{17}B_{1.0}$ melt-spun ribbon exhibited a high remanence of 65 emu/g and a coercivity of 2.0 kOe.

Keywords: Sm-Fe alloys; rare-earth magnet; melt-spinning; coercivity; microstructures

1. Introduction

The Sm_5Fe_{17} phase is a ferromagnetic phase in the binary Sm-Fe system [1,2]. It is a metastable phase and its formation has been reported only in sputtered films [3,4]. Through the intensive studies to produce the Sm_5Fe_{17} phase as bulk materials, it was found that the Sm_5Fe_{17} phase can be obtained by annealing of amorphous melt-spun ribbons [5]. Sm_5Fe_{17} melt-spun ribbon shows a large coercivity exceeding 25 kOe and a remanence of 40 emu/g, which is significantly lower than the remanence of Nd-Fe-B magnets. For the application in the motors of electric vehicles and

wind-turbine generators, the temperature of the magnets rises to nearly 473 K due to the evolution of eddy currents. Nd-Fe-B magnets cannot be used for the motors and instead Nd-Dy-Fe-B magnets, which the Dy was added to increase the coercivity, are applied. At such a high temperature, the magnetic properties of the Sm_5Fe_{17} melt-spun ribbon were almost comparable to those of the Nd-Fe-B melt-spun ribbon (The results are discussed later in the results and discussion section). Thus, the high coercivity magnets are required for the high temperature applications. Since the Sm_5Fe_{17} melt-spun ribbon possesses the high coercivity, it can be suitable for a hard magnet component in the nanocomposite magnets, which is the most promising candidate for the new types of the permanent magnets. In any case, the increase of the remanence of the Sm_5Fe_{17} melt-spun ribbon is almost always beneficial. There have been several efforts to increase the remanence of Sm_5Fe_{17}-type melt-spun ribbons, but the reported values are not yet satisfactory [6,7,8]. It is known that the magnetic properties of Sm-Co-based magnets can be improved by the addition of B to the Sm-Co-based alloy [9,10,11]. In this study, small amounts of B were added to Sm_5Fe_{17} melt-spun ribbon in order to increase the remanence. The structures and magnetic properties of the Sm-Fe and Sm-Fe-B melt-spun ribbons were then examined.

2. Materials and Method

Sm_5Fe_{17} and $Sm_5Fe_{17}B_x$ (x = 0.5–1.5) alloy ingots were induction melted in an argon atmosphere in a quartz crucible having an orifice of 0.6 mm in diameter at the bottom. The molten metal was ejected through the orifice with argon onto a chromium-plated copper wheel rotating at a surface velocity of 40 ms^{-1}. The resultant melt-spun ribbons were annealed under an argon atmosphere at temperatures between 773 K and 1073 K for 1 h. The phases in the specimens were examined by X-ray diffraction (XRD) using Cu Kα radiation. The microstructures of the specimens were examined using a transmission electron microscope (TEM) after ion beam thinning. The thermomagnetic properties of the specimens were examined in a vacuum using a vibrating sample magnetometer (VSM) with an applied field of 500 Oe. The magnetic properties of the specimens were measured by the VSM with a maximum applied field of 25 kOe after premagnetization in a pulsed field of 70kOe. Some of the specimens were further examined by VSM using a superconducting magnet with a maximum applied field of 100 kOe.

3. Results and Discussion

3.1. Sm-Fe melt-spun ribbon

The Sm_5Fe_{17} melt-spun ribbons were amorphous and exhibited a low coercivity value, less than 1 kOe. It is known that crystalline phases can be produced by rapid solidification processing and subsequent heat treatment [6]. In the previous studies [7,8], the annealed samples consisted of the Sm_5Fe_{17} phase but also contained some other phase such as the $SmFe_{12}$ phase and the $SmFe_3$ phase. As the result of the extensive study of the annealing conditions, the optimal annealing condition to obtain the Sm_5Fe_{17} phase was established in this paper. Figure 1 shows the XRD patterns of the annealed Sm-Fe melt-spun ribbons. The amorphous melt-spun ribbon should be annealed at relatively high heating rates of 0.5–1.0 K/s to 873–973 K and then kept for 1 h. As shown in Figure 1, the optimal annealed specimens consisted of the Sm_5Fe_{17} (hexagonal) phase. However, the Sm-Fe

ribbon annealed at 1073 K consisted of the $SmFe_3$ (rhombohedral) phase together with the Sm_5Fe_{17} phase.

Figure 2 shows the dependence of the coercivity of the Sm_5Fe_{17} melt-spun ribbons on the annealing temperature. The specimens annealed at 873 K and 973 K showed high coercivity values. According to the results of the XRD studies, those annealed melt-spun ribbon consists of the Sm_5Fe_{17} phase. This indicates that the observed high coercivity in the annealed melt-spun ribbon is due to the existence of the Sm_5Fe_{17} phase.

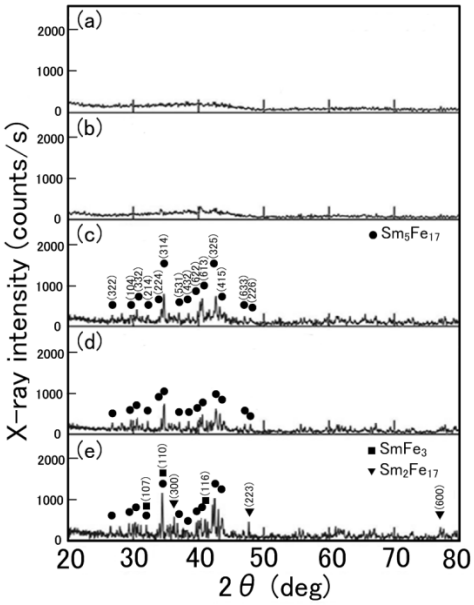

Figure 1. XRD patterns of (a) the Sm-Fe melt-spun ribbon and the specimens annealed at (b) 773 K, (c) 873 K, (d) 973 K, and (e) 1073 K.

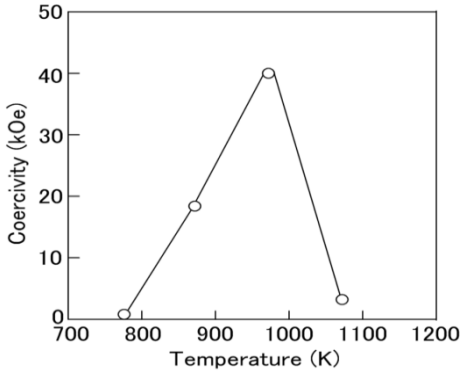

Figure 2. Dependence of the coercivity of the Sm-Fe melt-spun ribbons on the annealing temperature.

The hysteresis loops of the Sm_5Fe_{17} melt-spun ribbon and the specimen annealed at 973 K are shown in Figure 3. Since the applied field of 25 kOe is far lower than the field required to fully saturate the Sm_5Fe_{17} melt-spun ribbon, the hysteresis curve is not closed (i.e., it is a minor loop), and

it is not symmetrical with respect to either coordinate. The actual coercivity of the annealed specimen was measured as 40 kOe using a superconducting magnet with a maximum applied field of 100 kOe.

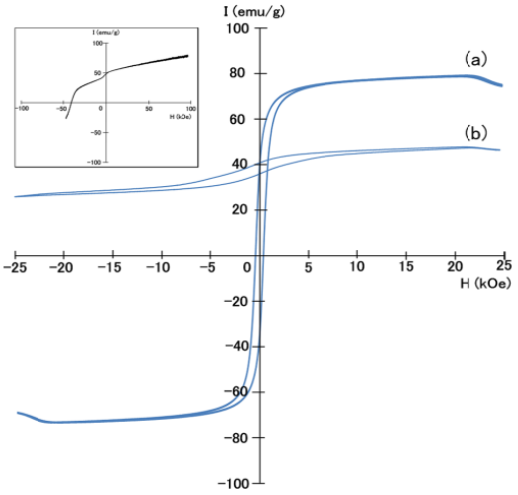

Figure 3. Hysteresis loops of (a) the Sm-Fe melt-spun ribbon and (b) the specimen annealed at 973 K. The demagnetization curve of the annealed specimen measured using a superconducting magnet with a maximum applied field of 100 kOe is also shown in the insert.

Figure 4 shows the hysteresis loops of the Sm_5Fe_{17} melt-spun ribbon and the $Nd_{15}Fe_{77}B_8$ melt-spun ribbon measured at 473 K under the applied magnetic field of 20 kOe. Although the Sm_5Fe_{17} melt-spun ribbon ribbons showed a much smaller remanence than the $Nd_{15}Fe_{77}B_8$ melt-spun ribbon at room temperature, it exhibits a much smaller difference in remanence at 473 K. Therefore, the magnetic properties of the Sm_5Fe_{17} melt-spun ribbon are comparable to those of $Nd_{15}Fe_{77}B_8$ melt-spun ribbon at 473 K.

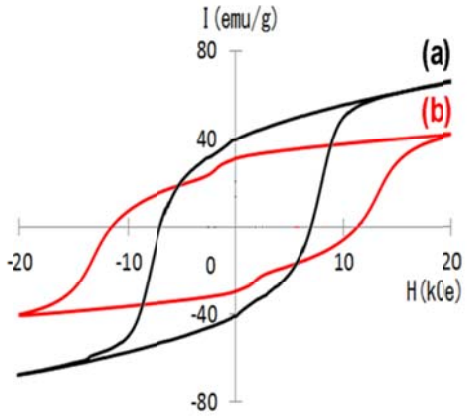

Figure 4. Hysteresis loops of (a) the $Nd_{15}Fe_{77}B_8$ melt-spun ribbon and (b) the Sm_5Fe_{17} melt-spun ribbon measured at 473 K. The high-temperature measurements were made by VSM under a maximum applied magnetic field of 20 kOe.

3.2. Sm-Fe borides

The $Sm_5Fe_{17}B_x$ (x = 0.5–1.5) melt-spun ribbon showed a low coercivity, as was the case for the Sm_5Fe_{17} melt-spun ribbon. Figure 5 shows the dependence of the coercivity of the $Sm_5Fe_{17}B_x$ (x = 0.5–1.5) melt-spun ribbons on the annealing temperature. The coercivity of the $Sm_5Fe_{17}B_x$ (x = 0.5–1.5) alloys shows a similar temperature dependence, but their maximum coercivity, achieved by annealing at 973 K, decreases with increasing B content of the alloy. This indicates that the addition of B to the Sm_5Fe_{17} alloy results in a decrease in coercivity.

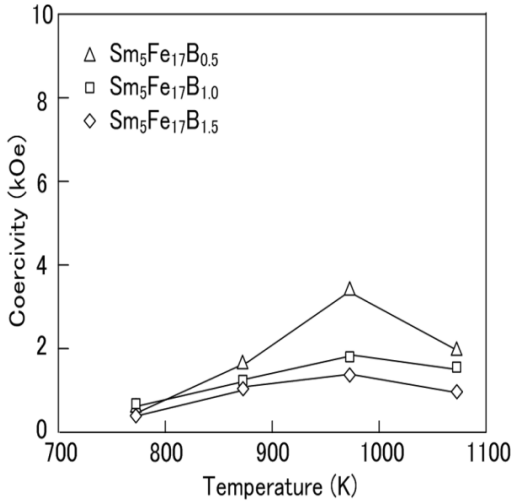

Figure 5. Dependence of the coercivity of the $Sm_5Fe_{17}B_x$ (x = 0.5–1.5) melt-spun ribbons on the annealing temperature.

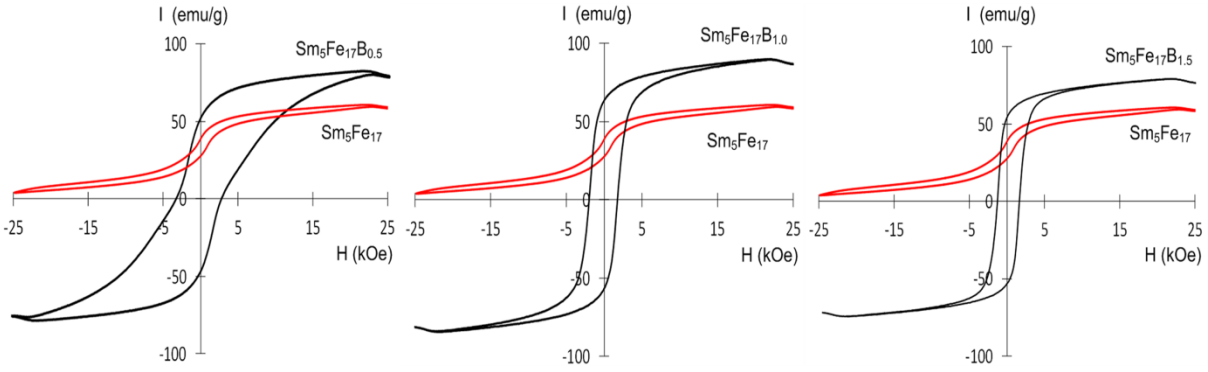

Figure 6. Hysteresis loops of the $Sm_5Fe_{17}B_x$ (x = 0.5–1.5) melt-spun ribbons annealed at 973 K. For comparison, the hysteresis loop of the Sm_5Fe_{17} melt-spun ribbon annealed at 973 K is also shown in the each figure.

Figure 6 shows the hysteresis loops of the $Sm_5Fe_{17}B_x$ (x = 0.5–1.5) melt-spun ribbons annealed at 973 K. For comparison, the hysteresis loop of the Sm_5Fe_{17} melt-spun ribbon annealed at 973 K is shown in the each figure. It is found that the remanence of the $Sm_5Fe_{17}B_x$ (x = 0.5–1.5) alloys is higher than that of the Sm_5Fe_{17} alloy even though the coercivity of the $Sm_5Fe_{17}B_x$ (x = 0.5–1.5)

alloys is much smaller than that of the Sm_5Fe_{17} alloy. The remanence increases with increasing B content from 40 emu/g for the Sm_5Fe_{17} alloy to 65 emu/g for the $Sm_5Fe_{17}B_{1.0}$ alloy and then decreases to 60 emu/g for the $Sm_5Fe_{17}B_{1.5}$ alloy. The remanence of 65 emu/g exhibited by the annealed $Sm_5Fe_{17}B_{1.0}$ alloy is much higher than that of the annealed Sm_5Fe_{17} melt-spun ribbon.

The Sm_5Fe_{17} and $Sm_5Fe_{17}B_x$ (x = 0.5–1.5) melt-spun ribbons annealed at 973 K were examined by XRD and thermomagnetic studies to evaluate the differences in the coercivity value. Figure 7 shows the XRD patterns of the annealed Sm-Fe-B melt-spun ribbons. The diffraction peaks of the Sm_5Fe_{17} alloy were determined to be the Sm_5Fe_{17} phase. Virtually the same XRD patterns were obtained from the $Sm_5Fe_{17}B_{0.5}$ alloy. This indicates that the small addition of B to the Sm_5Fe_{17} alloy did not alter the XRD pattern. On the other hand, the XRD pattern of the $Sm_5Fe_{17}B_{1.0}$ alloy is quite different from that of the Sm_5Fe_{17} alloy. The diffraction peaks of the Sm_5Fe_{17} alloy were determined to be the $Sm_2Fe_{14}B$ and $SmFe_2$ phases. The XRD pattern of the $Sm_5Fe_{17}B_{1.5}$ alloy is similar to that of the $Sm_5Fe_{17}B_{1.0}$ alloy, indicating that the $Sm_5Fe_{17}B_{1.5}$ alloy also consisted of the $Sm_2Fe_{14}B$ (tetragonal) and $SmFe_2$ (cubic) phases. These results reveal that the large addition of B to the Sm_5Fe_{17} alloy resulted in the formation of the $Sm_2Fe_{14}B$ and $SmFe_2$ phases instead of the Sm_5Fe_{17} phase, and hence the decrease in coercivity.

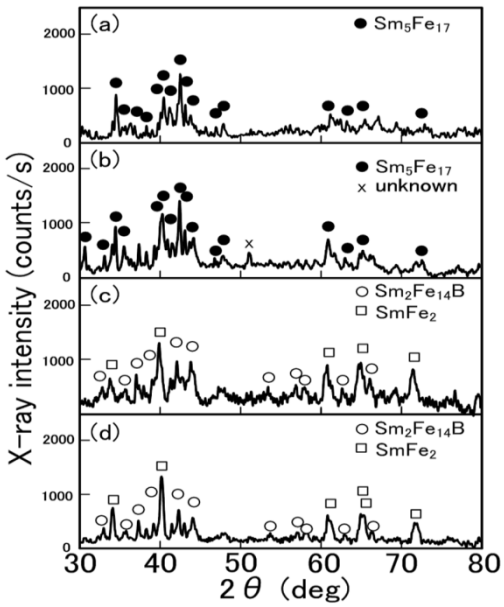

Figure 7. XRD patterns of the annealed melt-spun ribbons: (a) Sm_5Fe_{17}, (b) $Sm_5Fe_{17}B_{0.5}$, (c) $Sm_5Fe_{17}B_{1.0}$, and (d) $Sm_5Fe_{17}B_{1.5}$ alloys.

Figure 8 shows the thermomagnetic curves of the annealed Sm-Fe-B melt-spun ribbons. The thermomagnetic curve of the Sm_5Fe_{17} alloy exhibits one magnetic transition at around 550 K, which corresponds to the Curie temperature of the Sm_5Fe_{17} phase. Unlike in the case of the XRD studies, the thermomagnetic curve of the $Sm_5Fe_{17}B_{0.5}$ alloy is quite different from that of the Sm_5Fe_{17} alloy. The thermomagnetic curve exhibits three magnetic transitions at around 550 K, 620 K, and 680 K. It has been reported that the Curie temperatures of the $Sm_2Fe_{14}B$ phase and $SmFe_2$ phase are 616 K and 675 K, respectively [12,13,14]. Therefore, the $Sm_5Fe_{17}B_{0.5}$ alloy contains the $Sm_2Fe_{14}B$ and $SmFe_2$ phases together with the Sm_5Fe_{17} phase. The thermomagnetic curve of the $Sm_5Fe_{17}B_{1.0}$ alloy exhibits

two magnetic transitions at around 620 K and 680 K, indicating that the $Sm_5Fe_{17}B_{1.0}$ alloy has no Sm_5Fe_{17} phase. The $Sm_5Fe_{17}B_{1.5}$ alloy also exhibits two magnetic transitions at around 620 K and 680 K, which correspond to the Curie temperatures of the $Sm_2Fe_{14}B$ and $SmFe_2$ phases. This is consistent with the results of the XRD studies.

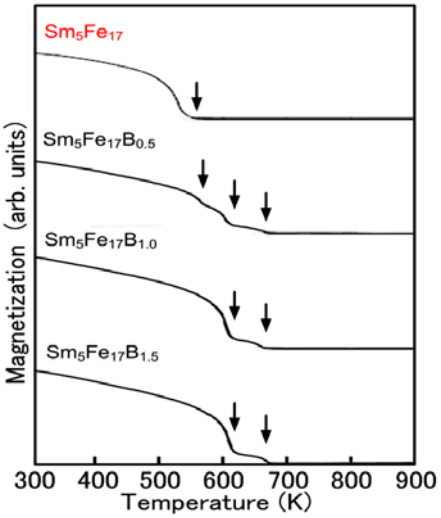

Figure 8. Thermomagnetic curves of the annealed Sm-Fe-B melt-spun ribbons.

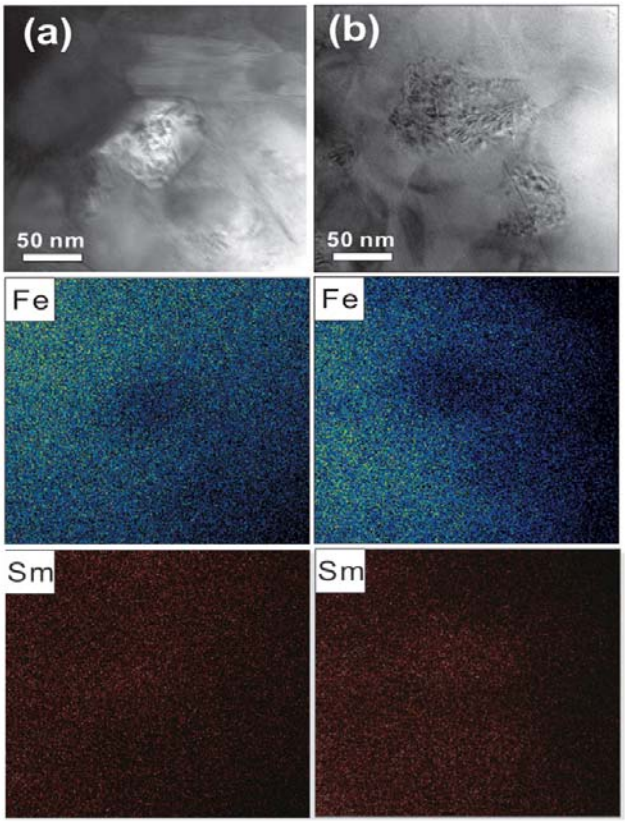

Figure 9. TEM micrographs of the (a) $Sm_5Fe_{17}B_{0.5}$ and (b) $Sm_5Fe_{17}B_{1.5}$ annealed melt-spun ribbons and corresponding X-ray mappings for iron and samarium.

Figure 9 shows TEM micrographs of the annealed $Sm_5Fe_{17}B_{0.5}$ and $Sm_5Fe_{17}B_{1.5}$ melt-spun ribbons. The grain size of the annealed $Sm_5Fe_{17}B_{0.5}$ alloy was around 50 nm in diameter, which is almost comparable to the reported grain size of annealed Sm_5Fe_{17} alloy [8]. Samarium and iron were detected in most of the grains of the annealed $Sm_5Fe_{17}B_{0.5}$ alloy, except for the centrally located grain that were rich in samarium but poor in iron. According to the results of the thermomagnetic studies, the specimens contained some of the $Sm_2Fe_{14}B$ (Sm11.7 at%) and $SmFe_2$ (Sm33.3 at%) phases together with the Sm_5Fe_{17} (Sm22.7 at%) phase. Thus, the samarium-rich centrally located grain consisted of the $SmFe_2$ phase and the surrounding grains were either the $Sm_2Fe_{14}B$ or Sm_5Fe_{17} phase. The upper-left grain region, which was rich in iron but slightly poor in samarium, may be the $Sm_2Fe_{14}B$ phase. In the TEM micrograph of the annealed $Sm_5Fe_{17}B_{1.5}$ alloy, an increase was seen in the amount of the $SmFe_2$ phase, where is poor in iron but rich in samarium. The grain size of the $SmFe_2$ phase was found to be larger than that in the annealed $Sm_5Fe_{17}B_{0.5}$ alloy. Since the $Sm_5Fe_{17}B_{1.5}$ alloy consisted of the $Sm_2Fe_{14}B$ and $SmFe_2$ phases, the surrounding grains are considered to be the $Sm_2Fe_{14}B$ phase. This confirms that the addition of B to Sm_5Fe_{17} alloy results in the formation of the $SmFe_2$ and $Sm_2Fe_{14}B$ phases, instead of the formation of a $Sm_5Fe_{17}B_x$ phase. Since the $Sm_2Fe_{14}B$ phase does not possess uniaxial anisotropy [12], the observed coercivity of the annealed Sm-Fe-B melt-spun ribbons is considered to be the fine $SmFe_2$ phase.

4. Conclusion

The structures and magnetic properties of $Sm_5Fe_{17}B_x$ (x = 0–1.5) melt-spun ribbons annealed at 973 K were examined. The annealed Sm_5Fe_{17} melt-spun ribbon consisted of the Sm_5Fe_{17} phase and exhibited a high coercivity. The annealed $Sm_5Fe_{17}B_{0.5}$ melt-spun ribbon consisted of the Sm_5Fe_{17} phase together with the $Sm_2Fe_{14}B$ and $SmFe_2$ phases. In contrast, the annealed $Sm_5Fe_{17}B_x$ (x = 1.0–1.5) melt-spun ribbons consisted of the $Sm_2Fe_{14}B$ and $SmFe_2$ phases. The coercivity of the annealed $Sm_5Fe_{17}B_x$ (x = 0–1.5) melt-spun ribbons decreased as the B content increased. On the other hand, the annealed $Sm_5Fe_{17}B_x$ (x = 0.5–1.5) melt-spun ribbons exhibited a higher remanence than the Sm_5Fe_{17} melt-spun ribbon.

Acknowledgments

The use of the facilities of the Materials Design and Characterization Laboratory at the Institute for Solid State Physics, the University of Tokyo, is gratefully acknowledged. This work was performed at High Field Laboratory for Superconducting Materials, Institute for Materials Research, Tohoku University.

Conflict of Interest

All authors declare no conflicts of interest in this paper.

References

1. Kamprath H, Liu NC, Hedge H, et al. (1990) Magnetic properties of Sm−Fe−Ti−Al sputtered films with $_iH_c$ greater than 30 kOe. *J Appl Phys* 67: 4948–4950.

2. Stadelmaier HH, Schneider G, Henig ETh, et al. (1991) Magnetic $Fe_{17}R_5$ in the Fe-Nd and Fe(-Ti)-Sm systems, and other phases in Fe-Nd. *Mater Lett* 10: 303–309.
3. Katter M, Wecker J, Schultz L, et al. (1990) Preparation of highly coercive Sm-Fe-Ti by rapid quenching. *Appl Phys Lett* 56: 1377–1379.
4. Cadieu FJ, Hegde H, Rani R, et al. (1991) Cell volume expansion in $Sm_5(Fe, T)_{17}$, T = Ti, V, magnetic phases. *Mater Lett* 11: 284–285.
5. Saito T, Ichihara M (2007) Synthesis and magnetic properties of Sm_5Fe_{17} hard magnetic phase. *Scripta Mater* 57:457–460.
6. Saito T (2007) Synthesis and magnetic properties of $(Nd_{1-x}Sm_x)_5Fe_{17}$ (x = 0–1) phase. *Appl Phys Lett* 91: 072503-1-072503-3.
7. Saito T (2007) High coercivity in Sm_5Fe_{17} melt-spun ribbon. *J Alloys Compd* 440: 315–318.
8. Saito T, Miyoshi H, Hamane DN (2012) Structures and magnetic properties of Sm_5Fe_{17} melt-spun ribbon. *J Appl Phys* 111: 07E322-1-07E322-3.
9. Kim DH, Zhang Y, Hadjipanayis GC (1998) Magnetic properties of Sm–Co–B-based nanocomposite magnets. *J Magn Magn Mater* 190: 302–306.
10. You C, Zhang ZD, Sun XK, et al. (2001) Phase transformation and magnetic properties of $SmCo_{7-x}B_x$ alloys prepared by mechanical alloying. *J Magn Magn Mater* 234: 395–400.
11. Gapalan R, Xiong XY, Ohkubo T, et al. (2005) Nanoscale microstructure and magnetic properties of melt-spun $Sm(Co_{0.725}Fe_{0.1}Cu_{0.12}Zr_{0.04}B_{0.015})_{7.4}$ ribbons. *J Magn Magn Mater* 295: 7–20.
12. Herbst JF (1991) $R_2Fe_{14}B$ materials: Intrinsic properties and technological aspects. *Rev Mod Phys* 63: 819–898.
13. Buschow KHJ (1971) The samarium-iron system. *J Less-Common Metals* 25: 131–134.
14. Kim HT, Xiao QF, Zhang ZD, et al. (1997) Phases of melt-spun $Sm_{1-x}Fe_{7+x}$ alloys and magnetic properties of their nitrides. *J Magn Magn Mater* 173: 295–301.

AIMS Press